

# FM spectroscopy in recoil-induced resonances

M C Fischer, A M Dudarev, B Gutiérrez-Medina and M G Raizen

Department of Physics, The University of Texas at Austin, Austin, Texas 78712-1081, USA

E-mail: raizen@physics.utexas.edu

Received 6 June 2001

Published 1 August 2001

Online at [stacks.iop.org/JOptB/3/279](http://stacks.iop.org/JOptB/3/279)

## Abstract

We report on an experimental study of recoil-induced resonances as a method of velocimetry for cold atomic samples. We present a refined experimental method that greatly improves the sensitivity of the measurement over previous experiments. Using frequency-modulation (FM) spectroscopy techniques we achieve a sensitivity that approaches the shot noise limit. In addition, we present a novel approach to deriving the line shape of the observed signal, based on the concept of quantum transport and tunnelling in motional Bloch bands.

**Keywords:** Ultra-cold atoms, FM spectroscopy, recoil-induced resonances, optical lattices

## 1. Introduction

The system of ultra-cold atoms in external potentials has become a model system in an increasing number of disciplines, such as condensed matter physics and nonlinear dynamics. Studying the evolution of the spatial and momentum distribution of an atomic ensemble can reveal information about many aspects of the system. *In situ*, non-destructive methods are desired in order to follow the evolution of the distributions without severely perturbing the sample. Spatial information can be obtained in such a way by dispersive imaging of the atomic ensemble [1]. Momentum distributions are commonly recorded using time-of-flight or ballistic expansion methods. A more complicated high-resolution method by measurement of the spatial correlation function has been demonstrated recently [2]. A common drawback of these measurement techniques is the alteration of the spatial distribution due to ballistic expansion of the atoms. Momentum distributions have also been recorded using velocity selective Raman transitions between internal atomic states [3]. During this measurement a part of the momentum distribution is selectively transferred to a different atomic state and detected destructively. All of these measurement techniques preclude a repeated measurement of the dynamics of an atomic sample without destroying it.

The method of recoil-induced resonances (RIR) as a means of measuring the momentum distribution has been proposed and treated theoretically in [4, 5]. This method is based on stimulated photon scattering by atoms in an optical

lattice. An atom, changing its momentum due to the interaction with the optical lattice, will cause a corresponding change of the number of photons in the constituent light beams. One can measure this change of optical power in order to obtain information about the momentum distribution of the atoms.

RIR measurements of the momentum distribution have been reported in cold samples of alkali atoms [6–9]. However, these experiments were performed close to atomic resonance, resulting in a large distortion due to spontaneous scattering. The atomic cloud was pushed away entirely during the interaction and for a subsequent measurement the sample had to be prepared again. In response to this limitation, we have developed a refined method that greatly improves the sensitivity of the measurement. This method employs frequency-modulation (FM) spectroscopy techniques and is ultimately limited by intrinsic shot noise in the interaction probe beams.

The paper is organized as follows. In section 2 we briefly review the fundamental properties of RIR in the quantum optics picture. We derive in section 3 the properties of RIR based on the framework of quantum transport and tunnelling in motional Bloch bands. In section 4 we describe the experimental apparatus, focusing on the implementation of the FM technique. Finally, in section 5 we discuss the experimental results and point out the fundamental limitations of the method.

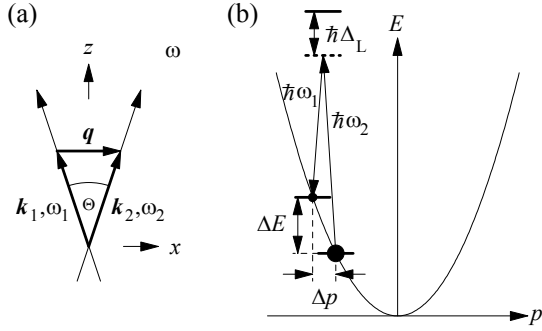


**Figure 1.** (a) Sketch of the beam arrangement for the recoil-induced resonance experiments. (b) Stimulated Raman transition between motional states of an atom. For a given frequency difference between the beams two velocity classes are coupled by the Raman process. The resonant velocity classes are determined by energy and momentum conservation laws.

## 2. Quantum optics approach

Our system consists of cold atoms illuminated by two far-detuned laser beams. The beams intersect at the position of the atomic cloud with a small enclosed angle  $\Theta$  as indicated in figure 1(a). An atom can undergo a stimulated Raman transition between motional states, as illustrated in figure 1(b), during which it transfers a photon from one light beam to the other. If the detuning  $\Delta_L$  of the beams from atomic resonance is sufficiently large, the probability of spontaneous scattering is negligible.

For the transfer of a photon between the beams, momentum conservation leads to a change in atomic momentum of

$$\Delta p = p_{\text{final}} - p_{\text{initial}} = \hbar k_2 - \hbar k_1 \equiv \hbar q, \quad (1)$$

where  $k_i$  denotes the wave vector of the travelling light waves with  $k_2 \approx k_1 \equiv k_L$ . For small angles the absolute value of the momentum difference  $\hbar q$  can be significantly smaller than the single photon recoil momentum  $\hbar k_L$ . The condition for energy conservation reads

$$\Delta E = \frac{p_{\text{final}}^2}{2M} - \frac{p_{\text{initial}}^2}{2M} = \hbar \delta, \quad (2)$$

where  $\delta = \omega_2 - \omega_1$  is the frequency difference between the two beams. We assume that the beams propagate in the  $x$ - $z$  plane, as indicated in figure 1(a). The momentum difference  $q$  is then

$$q = q_x = 2k_L \sin \frac{\Theta}{2}. \quad (3)$$

Combining equations (1) and (2) results in

$$v \cdot q = v_x q = \delta - \frac{\hbar q^2}{2M}. \quad (4)$$

For small angles we neglect terms of second order in  $q$

$$\delta = \frac{p_x q}{M}. \quad (5)$$

This equation constitutes a resonance condition for the stimulated Raman process. By choosing  $\delta$  appropriately, we

can select a subset of the atomic ensemble with momentum  $p_x$  that will undergo a stimulated Raman transition. From equation (4) it is apparent that only the velocity component along the  $x$ -direction is relevant, therefore, we will restrict our analysis to one dimension.

### 2.1. Quasi-static solution

For a given frequency difference  $\delta$ , atoms can change their momentum resonantly from  $p_x$  to  $p_x + \hbar q$ . During this process one photon is transferred from the pump beam (frequency  $\omega_1$ ) to the probe beam ( $\omega_2$ ). The reverse process can also occur, where a photon is transferred from the probe to the pump beam. Depending on the initial population of the two momentum states  $p_x$  and  $p_x + \hbar q$ , a net gain or loss in the probe beam results.

Integrating over a distribution of particles that transfer momentum, a scattering rate of photons  $W$  between the beams can be calculated as [4, 5]

$$W = N \frac{\pi}{2} \Omega_R^2 \hbar M \left. \frac{\partial \Pi}{\partial p} \right|_{p=\frac{M\delta}{q}}, \quad (6)$$

assuming a momentum distribution function  $\Pi(p)$ . In this equation  $N$  is the number of atoms, each having mass  $M$ , and  $\Omega_R$  is given by

$$\Omega_R = \frac{\Omega_1 \Omega_2}{2\Delta_L}, \quad (7)$$

where  $\Omega_i = d \cdot E_i / \hbar$  is the resonant Rabi frequency for each beam.

### 2.2. Extension for changing frequency

The derivation of equation (6) assumed that the frequency difference  $\delta$  between the beams is not changing with time. In the experiment we linearly chirp  $\delta$  in order to sweep the resonance condition for the Raman process through the entire distribution. We can estimate conditions for the chirp rate under which the result in equation (6) is still applicable.

In order to resolve a resonance of width  $\Delta\omega$  with a chirped frequency probe, the time during which the frequency has to hover in the range of the Raman resonance needs to be larger than  $\Delta t = 2\pi / \Delta\omega$ . During a linear scan  $\delta = rt$  the frequency stays in the range  $\Delta\omega$  for a time of  $\tau = \Delta\omega / r$ . Setting  $\tau = \Delta t$  gives an expression for the maximum scan rate  $r_{\text{max}} = \frac{1}{2\pi} \Delta\omega^2$  which scales as the square of the Raman resonance width to be resolved. Utilizing equation (5), the maximum scan rate to resolve a momentum distribution of width  $\Delta p$  is therefore

$$r_{\text{max}} \approx \frac{1}{2\pi} \left( \frac{q \Delta p}{M} \right)^2. \quad (8)$$

It is clear from this scaling that for the measurement of distributions with decreasing widths, increased measurement times must be accepted, even though the range of momenta to be sampled is decreasing. For scan rates much faster than  $r_{\text{max}}$  the rate equation approximation made in the derivation of equation (6) no longer holds, and very complicated coherent dynamics of the system are to be expected.

Very small scan rates violate another approximation that is used in the derivation leading to equation (6). It was

assumed that the measurement process does not change the given momentum distribution function  $\Pi(p)$ . Even though the change in momentum for each photon transfer is very small for a small angle between the beams, it is always present. The time scale over which the population of coupled momentum states changes is the inverse Rabi frequency  $\Omega_R^{-1}$ . If, during the scan, the frequency remains in the vicinity of the Raman resonance much longer than the inverse Rabi frequency, a substantial alteration of the momentum distribution is to be expected. The width of the resonance can be estimated to be the frequency difference between two successive resonant Raman transitions. Setting  $\Delta p = \hbar q$  in equation (5) yields a width of

$$\Delta\delta = \Delta p \frac{q}{M} = \frac{\hbar q^2}{M}. \quad (9)$$

The time  $\Delta t$  during which the frequency hovers in this range should be much less than the inverse resonant Rabi frequency. A linear scan in frequency  $\delta = rt$  therefore leads to a condition for the minimum scan rate

$$r_{\min} \approx \frac{\hbar q^2}{M} \Omega_R. \quad (10)$$

For scan rates much slower than  $r_{\min}$  the momentum distribution will be dynamically changed during the measurement to such an extent as to change the outcome of the measurement itself. This is not to be confused with the heating of the atomic sample due to spontaneous scattering. The change of the momentum distribution described here is inherent to the measurement process and will occur even in the absence of spontaneous scattering.

### 3. Quantum transport approach

It is instructive to derive equation (6) using the framework of tunnelling between motional Bloch bands. A recent review of the analogies of our system to the system of electrons in a crystal lattice is given in [10].

To begin the analysis, we consider the interaction beams to form an interference pattern in the crossing region leading to an optical potential of the form  $\hbar\Omega_R \cos(qx - \delta t)$ . The lattice is turned on at a large negative velocity and is decelerated during the frequency scan towards the Raman resonance condition for  $p = 0$  at zero velocity. Then it is accelerated to a positive velocity as the scan continues. A sketch of the atomic motion through reciprocal space in the accelerated frame of reference is shown in figure 2. At the time the optical potential is turned on, the atoms have a large velocity compared to the well. They are therefore projected into bands with high band indices. The initial deceleration of the potential well moves the atomic distribution through reciprocal space towards lower energy (i.e. lower band indices). In doing so the atoms must tunnel through many band gaps. For the parameters used in the experiment, the higher band gaps are so small that the probability for tunnelling is essentially unity. During the tunnelling no photon transfer occurs between the beams. However, as the atoms approach the lowest band they can undergo Bragg reflection at the first band gap. In this case the atom removes a photon from one beam and transfers it into the other upon entering the first Brillouin zone. As the optical potential crosses the point

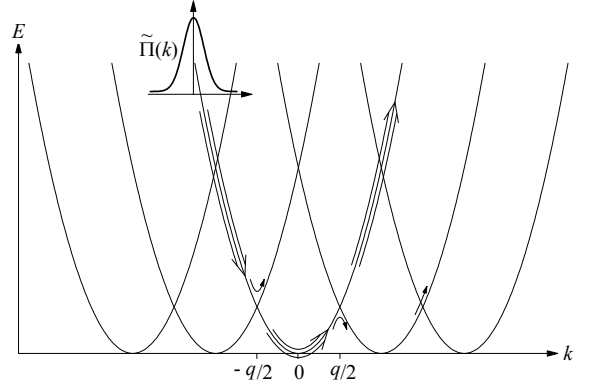


**Figure 2.** Sketch of the dynamics of the atomic motion through reciprocal space. The atomic ensemble starts out in high bands and approaches the lowest band. At the first band gap there is a small probability of undergoing a Bragg reflection, resulting in a change of momentum of  $+\hbar q$ . Most of the atoms, however, tunnel through the gap and transit the Brillouin zone in the lowest band. Upon exiting the zone they can Bragg reflect again back into the first band, changing their momentum by  $-\hbar q$ . The remaining atoms then continue their path towards higher band indices.

of zero velocity the atoms get transported back to higher band indices.

To simplify the analysis we assume that the majority of atoms tunnel through the lowest band gap and only few undergo a Bragg reflection. This assumption is justified for a large enough acceleration and a small enough well depth. The probability of tunnelling from the second into the first band upon entering the first Brillouin zone is equal to the probability of tunnelling back into the second band when leaving the Brillouin zone. Therefore only few atoms will Bragg reflect back into the first band after traversing the Brillouin zone. Extended Bloch oscillations of the atoms within the lowest band can be neglected due to the small reflection probability at the first band gap. This condition also ensures that the momentum distribution is not changed significantly during the interaction. The Bragg scattering process transfers a photon in opposite directions for scattering into and out of the first band. The total photon transfer rate is therefore the difference in the rate of scattering at the edges of the first Brillouin zone.

Let  $\Pi(p)$  denote the normalized momentum distribution of the atomic ensemble. As we know from the semi-classical equations of motion of a particle moving in a periodic potential [11], the quasi-momentum  $k$  varies linearly in time under the influence of a constant acceleration

$$k(t) = k_0 - \frac{1}{\hbar} Mat. \quad (11)$$

Transforming the stationary momentum distribution  $\Pi(p)$  into the quasi-momentum distribution in the accelerated frame  $\tilde{\Pi}(k, t)$  yields

$$\tilde{\Pi}(k, t) = \hbar \Pi(\hbar k + \hbar k(t)) = \hbar \Pi(\hbar k + [p_0 - Mat]), \quad (12)$$

with the normalization  $\int \tilde{\Pi}(k, t) dk = \int \Pi(p) dp = 1$ . The quantity we need to calculate is the number of particles per unit time undergoing a Bragg reflection at the first band gap. The rate of Bragg scattering upon entering the first Brillouin zone

$n^-$  is given by the rate of particles approaching that region multiplied by the probability to follow the band adiabatically instead of tunnelling through the gap. If we let  $P$  be the probability of tunnelling, then the probability of following the band adiabatically is  $1 - P$ . The scattering rate  $n^-$  is then

$$n^- = N \tilde{\Pi}\left(-\frac{q}{2}, t\right) \frac{dk}{dt} \cdot (1 - P), \quad (13)$$

where the quasi-momentum distribution is evaluated at the left edge of the Brillouin zone, and  $N$  is the total number of atoms participating. The Landau-Zener expression for the probability of tunnelling  $P$  is given by [12]

$$P = e^{-a_c/a}, \quad (14)$$

where the critical acceleration  $a_c$  for the first band gap is [13, 14]

$$a_c = \frac{\pi}{4} \frac{E_{\text{gap}}^2}{\hbar^2 k_L \sin \frac{\Theta}{2}}. \quad (15)$$

The factor of  $\sin(\Theta/2)$  takes into account the angled beam configuration, as opposed to the case of counterpropagating beams. The width of the first band gap  $E_{\text{gap}}$  is, to first order, [13]

$$E_{\text{gap}} = \hbar \Omega_R, \quad (16)$$

which gives for the critical acceleration

$$a_c = \frac{\pi}{2} \frac{\Omega_R^2}{q}. \quad (17)$$

For large acceleration we can write

$$n^- = N \tilde{\Pi}\left(-\frac{q}{2}, t\right) \frac{dk}{dt} \cdot (1 - e^{-a_c/a}) \quad (18)$$

$$= N \frac{\pi}{2} \frac{M}{q} \Omega_R^2 \Pi\left(-\frac{\hbar q}{2} + p_0 - Mat\right), \quad (19)$$

where we approximated  $1 - e^{-a_c/a}$  as  $a_c/a$ . Since each atom undergoing Bragg reflection at the first band gap transfers one photon, the photon scattering rate  $W^-$  is equal to the atomic Bragg scattering rate  $n^-$ . The total photon transfer rate  $W$  is the difference in the rate of scattering at the left ( $W^-$ ) and the right ( $W^+$ ) edge of the first Brillouin zone. Evaluating  $W^+$  in a similar manner we arrive at the expression

$$W = W^+ - W^- \quad (20)$$

$$= N \frac{\pi}{2} \hbar M \Omega_R^2 \left. \frac{\partial \Pi}{\partial p} \right|_{p=p_0 - Mat}. \quad (21)$$

In the last equation we approximated the difference term by a derivative, since for small angles the unit of momentum  $\hbar q$  is much smaller than the typical scale of variation of the momentum distribution. We can express the resonant momentum  $p$  in terms of the frequency difference between the beams, making use of the relation  $a = r/q$ :

$$p = p_0 - Mat = \frac{M}{q} (\delta_0 - rt) = \frac{M\delta}{q}. \quad (22)$$

This finally leads us to

$$W = N \frac{\pi}{2} \hbar M \Omega_R^2 \left. \frac{\partial \Pi}{\partial p} \right|_{p=\frac{M\delta}{q}}, \quad (23)$$

which is identical to equation (6) derived in the framework of Raman transitions.

## 4. Experimental realization

All experiments on recoil-induced resonances performed to date measured the momentum distribution of an atomic cloud by directly measuring the gain or absorption of one of the beams interacting with the cloud [6–9]. For this purpose the power  $P$  of the probe beam passing through the sample was recorded with a photodiode. The absorption coefficient

$$g \equiv \frac{P - P_0}{P_0} \quad (24)$$

was then determined by subtracting the value  $P_0$  for the impinging power from the signal and by subsequent normalization with  $P_0$ . Low-frequency noise and incomplete subtraction of the signals typically limit the resolution for the absorption coefficient of this set-up to about  $10^{-3}$ . This forced the experimenters to choose a small value for the detuning of the interaction beams from resonance in order to enhance the strength of the interaction. However, the drawback of doing so was a substantial number of spontaneous emissions.

### 4.1. Frequency-modulation spectroscopy

In order to enhance the sensitivity of the detection we used a frequency modulation set-up as sketched in figure 3. This method is commonly employed in high resolution spectroscopy [15]. The probe beam is phase modulated at a frequency  $\omega_m$ . The central frequency is chosen such that the frequency difference  $\delta$  between the first lower-frequency modulation sideband and the unmodulated pump beam is small. The amplitude  $E_i$  and intensity  $I_i$  of the incident probe beam are changed by the interaction with the atoms to

$$E_f = t(\delta) E_i \quad (25)$$

$$I_f = T(\delta) I_i. \quad (26)$$

These transmission coefficients are related to the gain coefficient by

$$T = t^2 = 1 + g. \quad (27)$$

Let us assume the momentum distribution to be measured has a width of order  $\Delta p$ . According to equation (5) the corresponding width of the distribution of resonance frequencies is  $\Delta\omega_{\text{res}} = (q/M)\Delta p$ . If the phase-modulation frequency  $\omega_m$  is chosen much larger than  $\Delta\omega_{\text{res}}$  then all but the first lower-frequency sideband of the probe beam are too far from the Raman resonance to be affected by the distribution. To analyse the resulting change of amplitude we can write the electric field of the incident modulated probe beam as

$$E_i = E_0 e^{i(\omega_0 t + m \sin(\omega_m t))} \quad (28)$$

$$= E_0 e^{i\omega_0 t} \sum_{n=-\infty}^{\infty} J_n(m) e^{in\omega_m t}, \quad (29)$$

where  $m$  is the modulation amplitude and  $J_n$  is the Bessel function of order  $n$ . Each frequency component is now amplified or attenuated according to the amplitude transmission coefficient  $t$  to form the final amplitude

$$E_f = E_0 e^{i\omega_0 t} \sum_{n=-\infty}^{\infty} t(\omega_0 + n\omega_m) J_n(m) e^{in\omega_m t}. \quad (30)$$

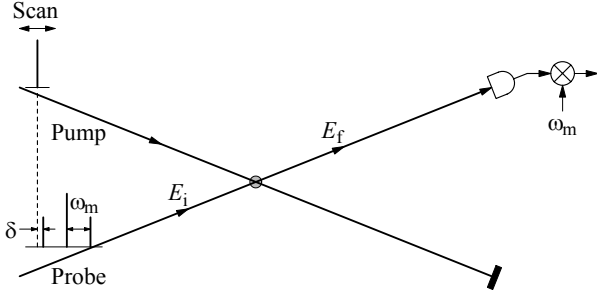


**Figure 3.** Sketch of the frequency modulation set-up to increase the detection efficiency. The probe beam is phase modulated at a frequency of  $\omega_m$ . The lower sideband has a frequency difference of  $\delta$  with respect to the pump beam. By linearly ramping the frequency of the pump beam,  $\delta$  is swept through the Raman resonance condition for atoms within the distribution. Frequency dependent absorption of the probe beam passing through the atoms causes an imbalance of the sideband intensities. The resulting intensity variations at the modulation frequency are detected by mixing the photodetector signal with the modulation drive.

The resulting intensity for the outgoing probe beam is

$$I_f = \frac{1}{2} c \epsilon_0 |E_f|^2. \quad (31)$$

In the absence of the atoms, the transmission coefficient is unity independent of the frequency, and the incident beam is unchanged ( $I_f = I_i$ ). If atoms are present, the transmission coefficients will lead to variations in the signal at the modulation frequency  $\omega_m$  and higher harmonics. The signal at the fundamental frequency  $\omega_m$  is given by

$$I_{\omega_m} = 2I_i \sum_k t(\omega_0 + k\omega_m) t(\omega_0 + [k-1]\omega_m) J_k J_{k-1}. \quad (32)$$

The value for  $t(\omega_0 + k\omega_m)$  is only appreciably different from unity if the frequency  $\omega_0 + k\omega_m$  is close to the frequency of the pump beam. As discussed above, only the first sideband fulfills this condition, so that  $t(\delta) = t(\omega_0 - \omega_m) \neq 1$  is the only term different from unity. Most terms in the sum cancel due to the property  $J_{-n} = (-1)^n J_n$  and the remaining terms leave us with

$$I_{\omega_m} = 2I_i [1 - t(\delta)] (J_0 J_1 + J_1 J_2) \quad (33)$$

$$= 2I_i [1 - t(\delta)] \frac{2}{m} J_1^2. \quad (34)$$

The factor  $(2/m)J_1^2(m)$  has its global maximum of 0.42 at  $m = 1.36$ .

The change of power in the probe beam due to gain or absorption in the atomic sample is given by

$$\Delta P_{\text{probe}} = \hbar \omega_0 W = g P_{\text{probe}}. \quad (35)$$

This gives an expression for the absorption coefficient  $g$

$$g = \frac{\hbar \omega_0}{P_{\text{probe}}} W. \quad (36)$$

For small values of  $g$  we see from equation (27) that  $1 - t \approx -g/2$ . The maximum change in the integrated power in the probe beam at the modulation frequency  $\omega_m$  is then

$$\Delta P_{\omega_m} = 0.42 \cdot 2P_{\text{probe}} [1 - t(\delta)] \approx -0.42 g P_{\text{probe}} \quad (37)$$

The maximum amplitude of the photocurrent signal corresponding to this change in power is

$$I_{\text{sig}} = \mathcal{R} \Delta P_{\omega_m} = 0.42 \mathcal{R} \hbar \omega_0 W, \quad (38)$$

where  $\mathcal{R}$  is the photodiode responsivity.

#### 4.2. Experimental set-up

In our experiment we started by trapping and cooling  $10^6$  sodium atoms in a magneto-optical trap (MOT). The atomic distribution was approximately Gaussian, with a width of  $\sigma_x = 0.35$  mm in position and  $\sigma_p = 8 \hbar k_L$  in momentum. At this point all the trapping and cooling fields were turned off and the interaction beams were introduced. The optical potential was turned on with a velocity corresponding to a value far outside the velocity distribution of the atomic ensemble. The frequency difference was then swept symmetrically through the resonance at a fixed rate, using an acousto-optic modulator (AOM).

As can be seen in figure 4, the frequency scanning arm of the set-up provided the pump beam. The centre frequency of the double pass AOM2 was 37.5 MHz and the scan range was typically  $\pm 450$  kHz. The beam was aligned through the position of the atomic cloud overlapping with the probe beam.

The fixed frequency arm of the set-up (probe beam) was phase modulated with an electro-optic modulator (EOM). The EOM operated at the optimum modulation index of  $m = 1.36$ , with a modulation frequency of 20 MHz. Because the first lower-frequency sideband was to be Raman-resonant with the atomic ensemble, the AOM in this path (AOM1) was operated at a frequency of 95 MHz. The optical axis of the EOM was aligned to minimize residual amplitude modulation (AM). After passing through the EOM the beam was aligned through the position of the atomic cloud overlapping with the pump beam. The angle between the beams was measured to be  $\Theta = 6.3^\circ$  and was dictated mainly by constraints of the vacuum chamber. After leaving the chamber the beam was focused onto a photodetector. As discussed previously, absorption or gain in the atomic sample leads to a signal component at the frequency of modulation  $\omega_m$ . In order to obtain a high signal-to-noise ratio the frequency dependent noise power density at the value for  $\omega_m$  should be as small as possible. The value  $\omega_m = 20$  MHz was chosen outside the range of significant electronic  $1/f$ -noise contributions while avoiding regions of increased noise due to other high frequency sources. Because the frequency of the signal to be recorded coincided with the frequency of the residual AM, a further reduction of this effect was necessary. For this purpose half of the power was split from the probe beam before entering the interaction region and both beams were directed onto the input ports of a balanced photoreceiver. Care was taken to equalize the beam intensities and the optical pathlength of both beams. The subtraction of the signals in the photodetector further reduced the AM contribution by 20 dB, suppressing it below the noise level. Noise measurements on the photodetector indicated that, at the maximum incident light power, the largest contribution to the noise is due to the shot noise of the incident light.

After being recorded by the photoreceiver, an RF mixer multiplied the amplified signal with a phase-shifted portion of the reference signal. The output was a DC level proportional

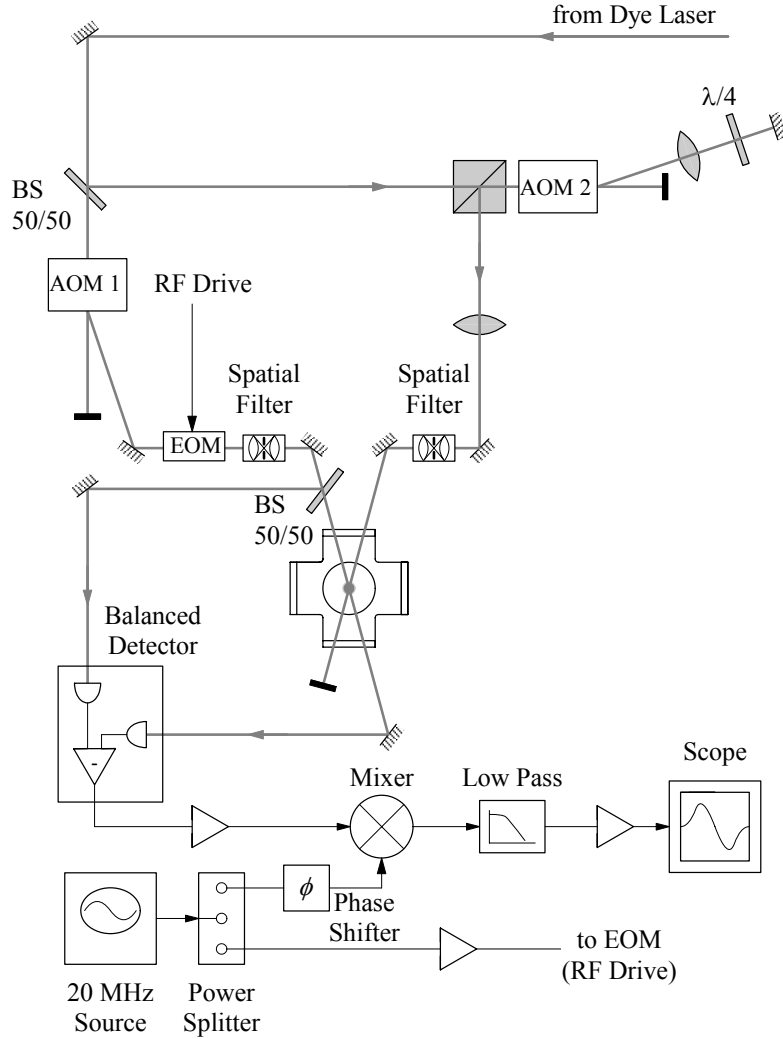


**Figure 4.** Sketch of the interaction beam set-up for the recoil induced resonance experiments. The frequency of the pump beam is adjusted by double-passing it through an acousto-optic modulator. An electro-optic modulator provides phase modulation sidebands on the probe beam. To cancel residual amplitude modulation, a balanced photoreceiver is used for detection. The recoil-induced resonance signal at the modulation frequency is extracted and captured on a digitizing oscilloscope for further analysis.

to the amplitude of the signal at the modulation frequency. Higher harmonics were eliminated by a low-pass filter with a cut-off frequency of 200 kHz. After a final amplification stage the signal was captured by a digitizing oscilloscope and transferred to the control computer for analysis.

## 5. Momentum measurements

Figure 5 shows an example of a single-shot, recoil-induced resonance trace. In this experiment an integrated power of  $P_{\text{pump}} = 5$  mW in the pump beam was focused onto the atoms. The spot size at the position of the atomic cloud was  $w_{\text{pump}} = 340$   $\mu\text{m}$ . The corresponding values for the probe beam were  $P_{\text{probe}} = 0.72$  mW and  $w_{\text{probe}} = 220$   $\mu\text{m}$ . The detuning from atomic resonance was  $\Delta_L/2\pi = 1$  GHz. The frequency difference of the two beams was scanned over 900 kHz in 200  $\mu\text{s}$ .

We can now compare the acquired signal to the theoretical approximation derived earlier. The initial condition of the atomic cloud before the RIR interaction was a Gaussian

distribution of momenta,

$$\Pi(p) = \frac{1}{\sqrt{2\pi}\sigma_p} \exp\left(-\frac{p^2}{2\sigma_p^2}\right), \quad (39)$$

with  $\sigma_p = 8\hbar k_L$ . This distribution had a size of roughly  $\sigma_x = 0.35$  mm and contained about  $1.5 \cdot 10^6$  atoms. The expression for the RIR signal in equation (6) is

$$W = N \sqrt{\frac{\pi}{8}} \Omega_R^2 \frac{1}{8\omega_r^2 \sin(\Theta/2)} \frac{\delta}{n_{\text{rec}}^3} \times \exp\left(-\frac{1}{2} \left(\frac{\delta}{4n\omega_r \sin(\Theta/2)}\right)^2\right), \quad (40)$$

where we expressed the width of the momentum distribution as  $\sigma_p = n_{\text{rec}}\hbar k_L$  and  $\hbar\omega_r$  is the single photon recoil energy. The maximum value  $W_{\text{max}}$  for the scattering rate in equation (40) occurs when the frequency difference has a value

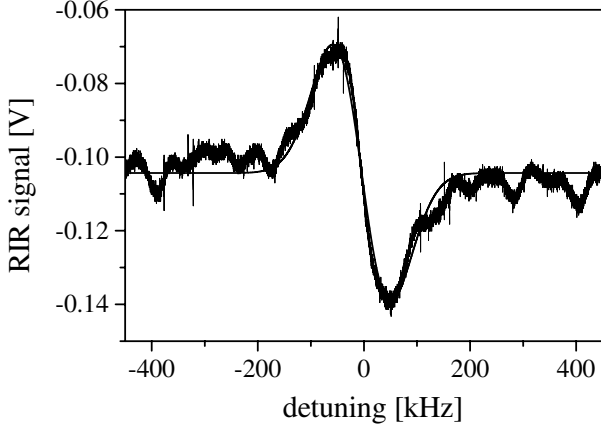


**Figure 5.** An example of a single-shot, recoil-induced resonance trace of the atomic distribution after being released from the MOT. Indicated also is a best fit of a derivative of a Gaussian curve to the experimental data. The fitted value for the width of the momentum distribution is  $\sigma_p = 10 \hbar k_L$ .

of  $\delta = q\sigma_p/M$ , resulting in

$$W_{\max} = N \sqrt{\frac{\pi}{8}} e^{-1/2} \Omega_R^2 \frac{1}{2n_{\text{rec}}^2 \omega_r}. \quad (41)$$

To optimize the RIR signal the interaction beam size should be comparable to the size of the atomic distribution. For much smaller beams only a fraction of the atoms interact with the light. Integration over the momentum distribution of width  $\sigma_x$ , taking into account the Gaussian profile of the beam intensity, decreases the maximum scattering signal by a factor

$$\eta_{\text{Gauss}} = \left( 1 + \frac{4\sigma_x^2}{w_{\text{probe}}^2} + \frac{4\sigma_x^2}{w_{\text{pump}}^2} \right)^{-1}. \quad (42)$$

Using equation (38) for the amplitude of the photocurrent signal at the modulation frequency yields

$$I_{\max, \text{rms}} = 0.42 \frac{1}{\sqrt{2}} \sqrt{\frac{\pi}{8}} e^{-1/2} N \eta_{\text{Gauss}} \mathcal{R} \hbar \omega_0 \Omega_R^2 \frac{1}{2n_{\text{rec}}^2 \omega_r}. \quad (43)$$

The photodiode used had a responsivity of  $\mathcal{R} = 0.4 \text{ A W}^{-1}$  and a transimpedance gain of  $700 \text{ V A}^{-1}$ . Tracing the electronic gain of the signal through the set-up resulted in a voltage gain of  $V_{\text{output}}/V_{\max, \text{rms}} \approx 1900$ . Combining equation (43) with the values for the experimental parameters yields an expected maximum change of power in the probe beam of  $\Delta P_{\text{probe}} = 0.4 \mu\text{W}$  and a corresponding signal of  $V_{\text{output}} = 60 \text{ mV}$ . The experimental trace has a maximum value of roughly  $V_{\text{output}} = 30 \text{ mV}$ . Considering the difficult calibration of the system and the strong dependence of the signal on the optical alignment the theoretical approximation agrees quite well with the experiment.

We can also obtain a theoretical value for the signal-to-noise ratio. The dominant noise source for the signal is the inherent fluctuation of the number of photons in the probe beam (shot noise). The noise current of the photodiode integrated over a bandwidth  $B$  is given by

$$I_{\text{noise}} = \sqrt{2eI_{\text{dc}}B}, \quad (44)$$

where  $e$  is the electron charge and  $I_{\text{dc}} = \mathcal{R}P_{\text{probe}}$  is the DC photocurrent. The integration bandwidth is determined by the low-pass filter in the electronic set-up and was set to  $B = 200 \text{ kHz}$ . Comparing  $I_{\text{noise}}$  to the value for the signal photo current in equation (43) leads to a signal-to-noise ratio of  $S/N \approx 15$ , which is not too far from the signal-to-noise ratio of the trace in figure 5.

Also indicated in figure 5 is a least-squares fit of a curve, as given in equation (40), to the experimental data. The best-fit value for the temperature of the atomic cloud was  $\sigma_p = 10 \hbar k_L$ . This value is slightly higher than the value  $\sigma_p = 8 \hbar k_L$  measured with the ballistic-expansion method. We attribute this to the measurement-induced heating described earlier.

To investigate this heating effect further we acquired RIR signals for various detunings of the interaction beams from resonance. Figure 6(a) shows the fitted value of  $\sigma_p$  in units of the single photon recoil momentum. For comparison, the horizontal line indicates the measurement of the initial temperature using the ballistic-expansion method. Part (b) of the same figure shows the fitted value for the amplitude of the RIR signal and the amplitude predicted from the theoretical approximation using equation (43).

It is important to note that for the RIR scans from which the data in figure 6 were obtained, the repump beam was left on during the interaction. For beam frequencies that were close to resonance for a particular hyperfine level of the ground state, the absence of the repump beam allowed the atoms to fall into the other hyperfine-ground state, for which the light was much further detuned. For detunings larger than roughly 1 GHz the presence of the repump beam did not change the RIR signal shape.

The dominant heating effect present in the experiments on RIR performed previously was the large number of spontaneous emissions during the interaction. In our experiment a ballistic-expansion measurement in the direction in which the RIR measurement was performed was not possible due to limited optical access for the imaging camera. To quantitatively study the amount of heating due to spontaneous emission, we determined the momentum that the atomic cloud acquired during the push. For this purpose we placed the imaging camera so that it was able to record the displacement of the atomic cloud in the direction of the interaction beams after a time of free expansion. The measurement of the mean acquired momentum in this direction enabled us to estimate the number of spontaneous emissions. Each absorbed photon leads to a momentum kick of  $\hbar k_L$  given to the atom. When an atom decays into the lower hyperfine ground state, it will immediately be pumped back to the excited state by the repump light. Since the repump beams illuminate the atomic sample from all directions, the absorption of photons from these beams does not lead to an average displacement of the cloud. However, this process will contribute to the heating of the sample. Assuming an isotropic emission we can then estimate the temperature increase due to the random-recoil momentum kicks. The temperature one could expect caused solely by this heating effect is indicated as a solid line in figure 6(a). One can see that the measured temperature increase can not be accounted for by spontaneous emission alone.

A few simple arguments can give us an estimate for the size of the heating effects. First we consider the heating inherent to

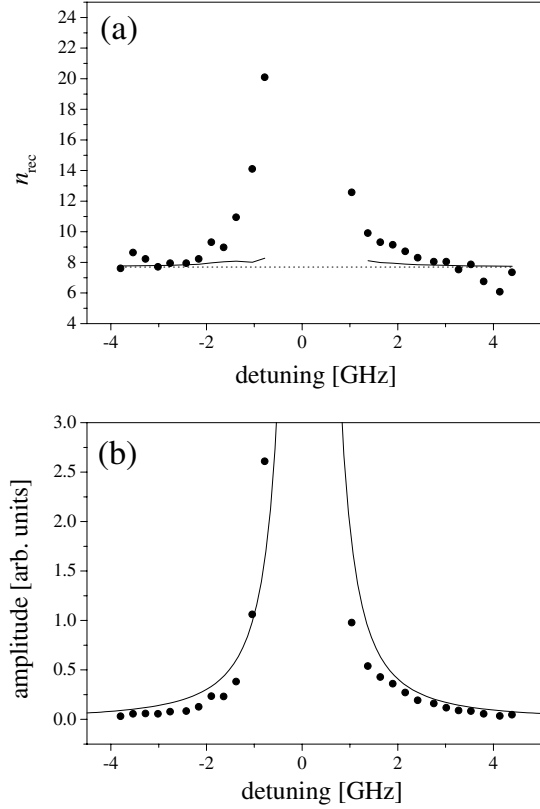


**Figure 6.** Dependence of the RIR signal parameters on the detuning of the interaction beams relative to the transition  $(S_{1/2}, F = 2) \rightarrow (P_{3/2}, F' = 3)$ . The data points in part (a) show the fitted value of  $n_{\text{rec}}$  ( $\sigma_p$  in units of the single photon recoil momentum). As a comparison the horizontal dotted line indicates the value for  $n_{\text{rec}}$  obtained with the method of ballistic expansion. The solid line indicates the momentum variance of the cloud that one could expect for the cloud being heated due to spontaneous emission alone. The data points in (b) show the fitted value of the amplitude. Indicated as a solid line is the dependence predicted from the theoretical approximation.

the measurement. The energy transferred to the atom during a single Raman transition is  $E = \hbar\delta$ . Integrating over the whole sweep duration yields the average energy transferred per atom:

$$E_{\text{inc,measure}} = \int W(\delta)dt = \frac{1}{r} \int W(\delta)d\delta \quad (45)$$

$$= \frac{4\pi}{r} \Omega_R^2 \hbar\omega_r \sin^2(\Theta/2). \quad (46)$$

This energy transfer leads to an increase in the momentum variance as

$$\sigma_{p,\text{final}}^2 = \sigma_{p,\text{initial}}^2 + 2ME_{\text{inc,measure}}. \quad (47)$$

The heating due to spontaneous emissions can be estimated by determining the spread in momentum caused by random emission of photons. Since we are only interested in the spread in one dimension, the increase in the variance after  $n_{\text{sc}}$  scattering events is [7]

$$\sigma_{\text{inc,spont}} = \frac{2}{3} \sqrt{n_{\text{sc}}} \hbar k_L. \quad (48)$$

The number of scattered photons can be estimated as

$$n_{\text{sc}} = 2 \cdot \left(\frac{\Gamma}{2}\right) \frac{S}{1 + S + 4(\Delta_L/\Gamma)^2} \cdot \tau_{\text{int}}, \quad (49)$$

where  $\tau_{\text{int}}$  is the duration of the interaction,  $\Gamma$  the excited state linewidth, and  $S$  the saturation parameter. The first factor of two in this equation accounts for the fact that photons can reach the lower hyperfine ground state. From there they are removed immediately by the repump beam, adding to the number of spontaneously scattered photons. For the parameters used to obtain the data in figure 6, the energy increase due to the measurement is about three times larger than the increase due to spontaneous emission for the range of detunings measured.

To test the limits of the semiclassical derivation given in section 2.2 we changed the scan rate of the frequency difference over a wide range. Experimental traces for the RIR signals for various scan rates are displayed in the left panel of figure 7. For all traces the scan direction was from negative to positive detunings. The estimates for the maximum and minimum scan rates as given by equations (8) and (10) for the parameters used in the experiments give  $r_{\text{min}} \approx r_{\text{max}} \approx (2\pi) \cdot 10 \text{ GHz s}^{-1}$ . This indicates a small range of scan rates for which the expression for the RIR signal is applicable.

For the top panel in figure 7, the scan rate was chosen much smaller than  $r_{\text{min}}$ . The trace shows a strong asymmetry in the shape. The first (positive) peak is large and localized whereas the second (negative) peak after the centre of the resonance is small and returns to zero very slowly with a long tail. The exchange of momentum within the atomic cloud always tends to increase the momentum spread of the distribution. At the start of the frequency scan the momentum is transferred from the central regions towards the wing in the direction opposite to the scan direction. For small scan rates the light interacts with a given velocity class for a long enough time to alter the distribution significantly. Off-resonant interactions let the atoms transfer momentum even before the light reaches the corresponding Raman resonance condition. This transfers most of the atoms prior to the frequency difference reaching zero for a resonance at  $p = 0$ . Past this point the momentum transfer occurs in the direction of the scan direction. The atoms which have not been transferred too far out of resonance can be ‘dragged’ along in the scan direction to very high momenta, explaining the long tail in the RIR signal trace. For the case of a fast scan (bottom panel) no such simple explanation could be found. The frequency is broadened substantially and the light is interacting with a large part of the ensemble simultaneously. The RIR traces show an oscillatory behaviour after the frequency passes through the resonance.

For illustrative purposes we compared the shape of the RIR signals to numerical quantum mechanical simulations. For the case of small angles in the RIR set-up the momentum quantization unit  $\hbar q$  was much smaller than the width in momentum of the real atomic sample. Therefore, numerical simulations with actual experimental parameters required the solution of a set of ordinary differential equations of prohibitively large dimension. Since we were not intending to extract quantitative information from the simulations, we restricted the simulation runs to distributions much narrower than the experimental ones. Because the scaling arguments for the scan rates involve the width of the distribution, the scan rates for the simulation had to be adjusted to reproduce the line shape observed in the experimental traces.

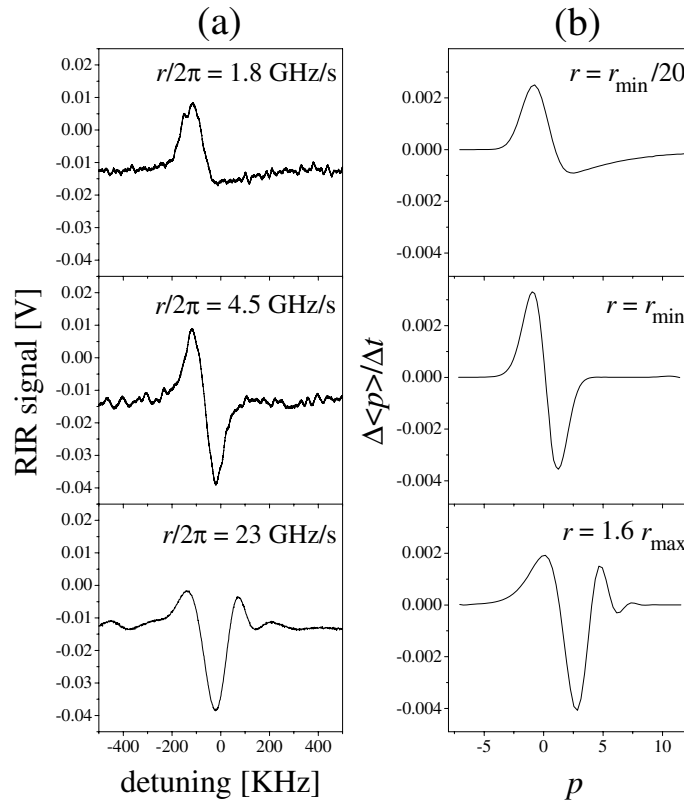


**Figure 7.** The left panel (a) shows experimental RIR traces for different scan rates. Each trace is an average over 20 acquisitions. The scan direction was from negative to positive detunings. The frequency range of the scan was held constant at  $\delta\nu = 900$  kHz, but the scan time was changed to produce the given scan rate. The right panel (b) shows quantum numerical simulations for scan rates that are smaller (top), within (middle) or outside (bottom) of the range  $[r_{\min}, r_{\max}]$ . It is important to point out that the parameters for the experimental runs and the numerical simulations are not the same, but illustrate qualitative agreement.

## 6. Conclusions

We have described an experimental set-up using frequency-modulation techniques that greatly enhances the sensitivity of the recoil-induced resonance method over previous experiments. We performed measurements that were limited by shot noise in the probe light. Heating due to spontaneous scattering was reduced below the level of the intrinsic measurement-induced heating. As a demonstration of this technique we extracted the temperature of an atomic sample from the signal line shape, but this technique can be used to characterize arbitrary momentum distributions. Due to its small perturbing effect on the atomic ensemble this technique can be used in applications where conventional (destructive) measurements cannot be applied.

## Acknowledgments

This work has been supported by the National Science Foundation, the Texas Advanced Research program, and the R A Welch Foundation.

## References

- [1] Andrews M R, Mewes M-O, van Druten N J, Durfee D S, Kurn D M and Ketterle W 1996 *Science* **273** 84
- [2] Saubaméa B, Hijmans T W, Kulin S, Rasel E, Peik E, Leduc M and Cohen-Tannoudji C 1997 *Phys. Rev. Lett* **79** 3146
- [3] Kasevich M, Weiss D S, Riis E, Moler K, Kasapi S and Chu S 1991 *Phys. Rev. Lett* **66** 2297
- [4] Guo J, Berman P R, Dubetsky B and Grynberg G 1992 *Phys. Rev. A* **46** 1426
- [5] Guo J and Berman P R 1993 *Phys. Rev. A* **47** 4128
- [6] Courtois J-Y, Grynberg G, Lounis B and Verkerk P 1994 *Phys. Rev. Lett.* **72** 3017
- [7] Meacher D R, Boiron D, Metcalf H, Salomon C and Grynberg G 1994 *Phys. Rev. A* **50** R1992
- [8] Guibal S, Triché C, Guidoni L, Verkerk P and Grynberg G 1996 *Opt. Comm.* **131** 61
- [9] Kozuma M, Imai Y, Nakagawa K and Ohtsu M 1995 *Phys. Rev. A* **52** R3421
- [10] Raizen M G, Niu Q and Salomon C 1997 *Physics Today* **50** 30
- [11] Ashcroft N W and Mermin N D 1976 *Solid State Physics* (Philadelphia: Saunders College)
- [12] Zener C 1932 *Proc. R. Soc. London A* **137** 696
- [13] Niu Q, Zhao X-G, Georgakis G A and Raizen M G 1996 *Phys. Rev. Lett.* **76** 4504
- [14] Bharucha C F, Madison K W, Morrow P R, Wilkinson S R, Sundaram B and Raizen M G 1997 *Phys. Rev. A* **55** R857
- [15] Hall J L, Hollberg L, Baer T and Robinson H G 1981 *Appl. Phys. Lett.* **39** 680